analytical chemistry

Article

pubs.acs.org/ac

Detection of Sugars via Chirality Induced in Europium(III) Compounds

Tao Wu,[†] Jiří Průša,[§,†] Jiří Kessler,[⊥,†] Martin Dračínský,[†] Jan Valenta,[*,‡] and Petr Bouř[*,†]

[†]Institute of Organic Chemistry and Biochemistry, Academy of Sciences, Flemingovo náměstí 2, Prague, 16610, Czech Republic

[§]Department of Analytical Chemistry, University of Chemistry and Technology, Technická 5, Prague, 16628, Czech Republic

[⊥]Department of Physical and Macromolecular Chemistry, Faculty of Science, Charles University, Hlavova 8, Prague, 12840, Czech Republic

[‡]Faculty of Mathematics and Physics, Charles University, Ke Karlovu 3, Prague, 12116, Czech Republic

Supporting Information

ABSTRACT: Detection and resolution of simple monosaccharides are difficult tasks because their structure is quite similar. The present study shows that circularly polarized luminescence (CPL) induced in europium complexes provides very specific spectral patterns for fructose, mannose, glucose, and galactose. Differences were also observed between bare Eu^{3+} ion and its complexes, when interacting with these sugars. The CPL spectra were measured on a Raman optical activity (ROA) spectrometer, which ensured high fluorescence intensity owing to the strong 532 nm laser excitation. The induced fluorescence was recorded in the same spectrum as the vibrational Raman bands. On the basis of the ligand field theory, most fluorescence spectral peaks could be assigned to *f*-shell europium transitions. Additional information on the interaction of the lanthanide with the sugar component was provided by measurement of time-dependent fluorescence, as formation of different complexes led to variations in fluorescence decay times. In nuclear magnetic resonance (NMR), the paramagnetic metal ion interacting with the sugars caused specific changes in ^{13}C chemical shifts. The spectroscopic data and molecular dynamics modeling showed that the interaction between the monosaccharides and Eu ion is rather weak due to the competition of the OH sugar groups with water molecules. However, multiple binding modes are possible, which contributes to the complexity and specificity of the spectra. The induced chirality and fluorescence spectra thus appear to be convenient means for monosaccharide detection and identification.

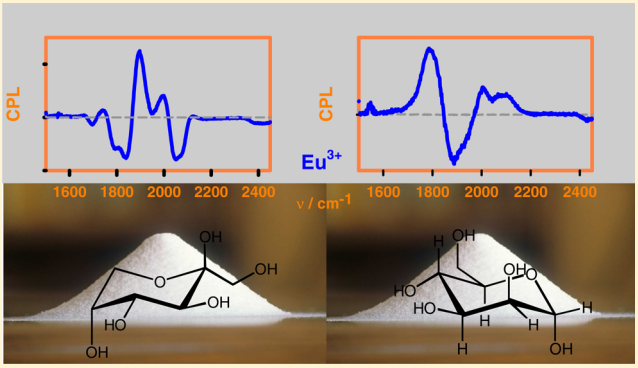

The prospect of detecting saccharides in physiologically relevant conditions attracts attention because it opens the way to monitoring and control of a wide range of biological processes including cellular recognition, immune response, and regulation of enzymatic activity. Metal coordination of natural carbohydrates in aqueous solution is particularly suitable for this purpose as it often provides remarkable selectivity and stability.[1−3] However, the stability of the complexes strongly depends on experimental conditions. A typical problem in detecting carbohydrates in an aqueous environment is a competition of the sugar receptor with the hydroxyl groups of water. Complexation of sugars with lanthanides can be followed by infrared or microwave spectroscopy where, however, rather unspecific changes were often observed.[3−5]

Fluorescence of the lanthanide complexes is much more sensitive even to weak interaction with saccharides and has been suggested to detect and identify neutral sugars including cancer biomarkers.[6] The interaction and specificity can be conveniently tuned by varying the metal and/or ligands.[3,7,8] For many metals and their complexes, the affinity to sugars and consequent stability constants are comparable to the older and still more common carbohydrate sensors based on the boronic acid.[9]

Circularly polarized luminescence (CPL), differential emission of the left- and right-circularly polarized light, is potentially even more attractive than the total luminescence, as CPL bands can be either positive or negative. CPL spectra are thus more specific, making it possible to distinguish more electronic transitions, and the information is easier to read. Lanthanide ions or their complexes are usually not chiral, but the chirality can be induced by the sugar component.[10,11] At the same time, the specific electronic structure of lanthanides[12] allows for a very high dissymmetry factor ($g = 2(I_R - I_L)/I$, i.e., twice the ratio of CPL to total luminescence, where I_R and I_L are the

Received: June 30, 2016
Accepted: August 15, 2016
Published: August 15, 2016

DOI: 10.1021/acs.analchem.6b02505
Anal. Chem. 2016, 88, 8878−8885

intensity of the right- and left-circularly polarized light, respectively).[13,14]

CPL measurements, however, are often difficult to do as sensitivity of CPL spectrometers is limited. In the present study, we use the Raman optical activity (ROA) spectrometer fitted with a strong 532 nm laser excitation source and a sensitive setup for detecting the difference in circular polarization.[15] This enables measurements of tiny CPL signals undetectable by other means.

Traditionally, the vibrational ROA spectroscopy detects a small difference in Raman scattering intensities of the right- and left-circularly polarized light.[16] It is sensitive to fine structural variations in chiral molecules and has been applied to a wide range of molecules including proteins, nucleic acids, and mono- and polysaccharides.[17−21] The ROA spectrum itself can thus be used as an extremely useful characteristic of the sugar. However, the ROA signal is often difficult to measure as well, because a typical circular intensity difference (CID, ratio of the ROA and Raman signal, i.e., the ROA analogy of g)[22] is very small, typically around 10^{-4}, and the Raman scattering itself is rather weak. High sugar concentrations are needed for a meaningful analysis.[23]

The CPL component of the ROA spectrum of europium−sugar conjugates measured together with the "true" vibrational ROA signal of pure sugars thus provides a welcome sensitivity enhancement of the spectroscopic detection. The interaction between the lanthanide or its complex and the monosaccharide provides an additional specificity about the sugar skeleton. The fluorescence bands are usually easily recognizable among the vibrational Raman and ROA bands in the spectrum, because of their higher intensity and stability of the lanthanide transition energies, only weakly dependent on the environment.[12] As previously discussed, the physical origin (fluorescence or Raman scattering) of the observed bands can also be unambiguously determined using multiple laser excitation wavelengths or by measuring the degree of circularity.[14]

In the present study, europium(III) in the form of chloride and two complexes stable in an aqueous environment are used to investigate the interaction with four common monosaccharides. The Eu^{3+} ion in particular provides a rich fluorescence spectrum within the wavelength range of the ROA spectrometer (about 532−610 nm). For mannose and fructose providing the strongest spectral responses, we correlate the CPL data to fluorescence decay times and paramagnetic nuclear magnetic resonance (NMR) shifts caused by the binding. A custom-made setup is used to record the fluorescence kinetics, as it is too slow (in the microsecond range) to be measurable on standard fluorescence spectrometers. The Eu−sugar interactions clearly bring about kinetics changes that are unreported so far to the best of our knowledge.

CPL induced in europium and other lanthanide complexes has been previously observed as a result of interaction with amino acids.[24−26] With the sugars, however, the interaction is much more specific. Early CPL studies were hampered by the limited sensitivity of available spectrometers[11] which restricted the number of systems that could be studied. For the amino acids, the induction of chirality was explained by a perturbed equilibrium of two enantiometric forms of the lanthanide (III) complexes. The ROA/CPL technique applied for sugars reveals greater variability and complexity of induced CPL spectra. At least to some extent, this could be explained by the multivalence modes possible for various sugar forms and rationalized by computational models involving density functional theory (DFT), molecular dynamics (MD), and the crystal field theory.

METHODS

The NaEuEDTA and Na_2EuDEPA complexes (Figure 1) were obtained by a reaction of europium oxide with 2.05 equiv of

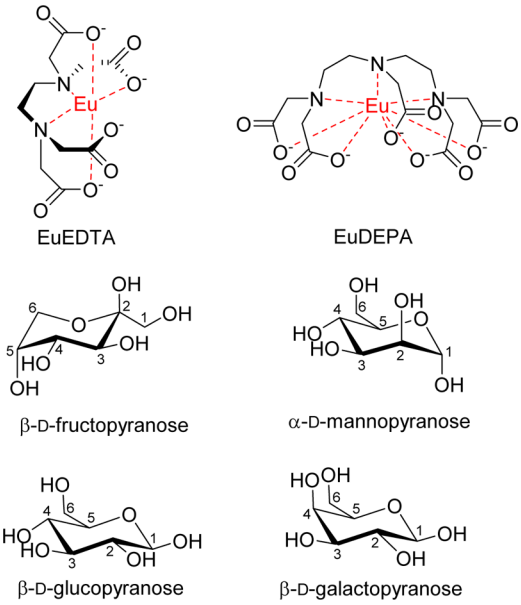

Figure 1. Structures of the two europium complexes and investigated monosaccharides. Monosaccharide forms most abundant in water solutions are depicted.

ethylenediaminetetraacetic (EDTA) and diethylenetriaminepentaacetic (DEPA) acid, respectively, kept in water at 70 °C for 4 h. The solution was then cooled down to room temperature, and the pH was adjusted to 7.0 by 1 M sodium carbonate solution. Water solutions of $EuCl_3$, NaEuEDTA, and Na_2EuDEPA complexes in 4 mM concentrations, and sugars (concentrations of 400−800 mM) were prepared, and their Raman and (back-)scattered circular polarized (SCP) ROA spectra were acquired on a BioTools spectrometer using 532 nm laser excitation, resolution of 7 cm^{-1}, laser power at the sample of 120−900 mW, and acquisition times of 1−16 h. Water background was subtracted from the Raman spectra; the water 1650 cm^{-1} band was also used to normalize the Raman intensities.

Fluorescence lifetimes were measured by a custom-build spectroscope (Charles University)[27] using epifluorescence illumination and collection of signal with an objective lens 4×/0.13 with a working distance of 17 mm. The continuous diode laser at 405 nm was modulated by a quartz acousto-optic modulator to provide square pulses with a repetition rate of 800 Hz and a 25% duty cycle. Typically, the pulse duration was 312.5 μs and the edge smearing was about 0.1 μs. Excitation power density in a solution measured inside a cuvette was about 0.8 W/cm^2. The fluorescence signal was verified to be a linear function of the excitation power. The signal was focused by a tube lens with focal length of 18 cm on an entrance slit of a grating spectrometer and detected by the Hamamatsu H11526-20-NF photomultiplier in the photon counting mode. Counts were treated with a multichannel scaler card MSA-300 (Becker & Hickl) set to 1200 points with 1 μs step. The signal was acquired during 1×10^5, 2×10^5, or 3×10^5 cycles. A second

DOI: 10.1021/acs.analchem.6b02505
Anal. Chem. 2016, 88, 8878−8885

output port of the spectrometer was equipped with a LN-cooled CCD camera which detected the fluorescence spectra.

NMR spectra were recorded at room temperature on a Bruker AVANCE III spectrometer operating at 500.0 MHz (^{1}H) and 125.7 MHz (^{13}C). About 16 mg of the monosaccharide was dissolved in 0.4 mL of D_2O and titrated by adding five times of 100 μL of $EuCl_3 \cdot 6H_2O$ (30 mg/0.6 mL) or EuEDTA (30 mg/0.6 mL) D_2O solutions. The spectra were referenced to C_6D_6, which was kept in a sealed capillary placed in the sample cuvette. 1D and 2D correlation NMR experiments (COSY, HSQC, HMBC) were combined to assign the signals.

The Gaussian[28] program was used to provide model geometries. X-ray geometries[29,30] of the NaEuEDTA and Na_2EuDEPA complexes were used as starting geometries and optimized by energy minimization using the B3LYP[31] functional, 6-311++G** basis set (the MWB28[32] pseudopotential and basis set for Eu), and polarizable continuum model (PCM)[33] for the water environment.

The semiempirical crystal field theory[12,34] was used to assign europium bands that are due to *f*-shell transitions and to approximately simulate the effect of the ligands. An adapted version of the Lanthanide[35] program was used in the calculation. As usual, the ligands were approximated by charge density computed on a grid using the Gaussian program, and the resultant electrostatic potential was used to perturb free ion energies and wave functions.[36−38]

For fructose and mannose, possible geometries and association energies of their complexes with the Eu^{3+} ion were also estimated using molecular dynamics simulations within the Amber program package.[39] In vacuum, a systematic search for the best binding sites was performed by minimizing the energy of a complex with the Eu^{3+} ion and the sugar, separately for α and β-anomers, and the furanose and pyranose fructose forms. About 200 positions of europium around the sugar were tested as the initial geometries; the minimization was performed with the GLYCAM06 force field[40] for the sugars; Eu^{3+} force field parameters were taken from ref 41. For all minima, the complexes were put into a cubic box ($(20\ Å)^3$) filled with 255 water molecules and molecular dynamics was run. For an equilibration phase (500 ps), the complex atoms were fixed and only water was allowed to relax, using the *nVT* ensemble, temperature of 300 K, and 1 fs integration time; then, the geometry was minimized again without any constraints. Free energies of the europium−sugar complex formation were estimated using the weighted histogram analysis method (WHAM).[42] Three characteristic Eu···O distances of the minimized structures were incremented by 0.25 Å, and the histograms were collected at 20 points, each of them containing 1 000 000 MD steps; the free energy profiles were obtained using the "Wham" script.[43]

RESULTS AND DISCUSSION

ROA and CPL Spectra. The spectra of the $EuCl_3$ and NaEuEDTA and Na_2EuDEPA aqueous solutions mixed with fructose, mannose, glucose, and galactose are plotted in Figure 2. Within the 200−1500 cm^{-1} interval, "ordinary" monosaccharide vibrational ROA spectra are apparent, as analyzed in other studies.[20,44−47] The ratio of the ROA and Raman signals (CID, circular intensity difference) is rather weak, and a relatively high noise level is present. Corresponding Raman spectra and ROA peak positions are plotted in Figure S1.

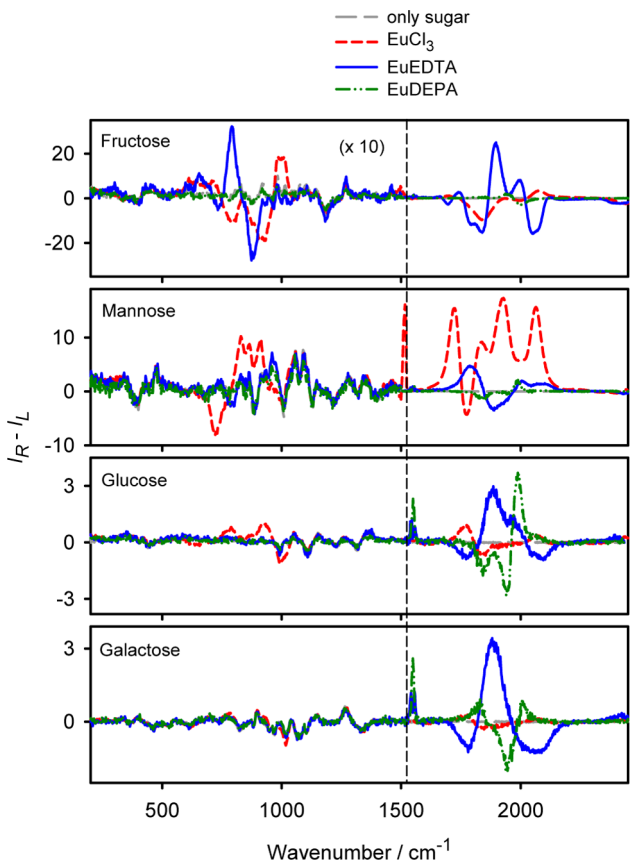

Figure 2. ROA spectra of $EuCl_3$, NaEuEDTA, and Na_2EuDEPA solutions in the presence of four monosaccharides exhibit a strong circularly polarized fluorescence component (right-hand side), very specific for each of the studied sugars.

An addition of the europium compounds is occasionally accompanied by the appearance of new bands within the 700−1000 cm^{-1} interval, intensity and CID of which is comparable with that of pure sugars. Much stronger bands appear within 1500−2450 cm^{-1}. These can be assigned to europium CPL and are more than ten times stronger than the vibrational ROA signal; it is thus much easier to measure them, and the signal-to-noise ratio is higher. Note that the noise level of both the Raman and ROA signal is proportional to the square root of the Raman counts on the detector.[16] Thus, the stronger signal of Raman/luminescence scattering also improves the accuracy of the ROA/CPL component. This is critical, for example, in a quantitative analysis for sugar mixtures.[20,23]

A closer look reveals remarkable specificity and significant differences among both the europium compounds and the sugars. For example, fructose induces a strong multiband pattern in the EuEDTA ion with peaks at 1696(−), 1746 (+), 1780 (−), 1839(−), 1897 (+), 1999 (+), 2052 (−), 2133 (+), and 2416 (−) cm^{-1}. The last band (2416 cm^{-1}) is close to the operational limit of the spectrometer, and its intensity might be attenuated by the limited sensitivity of the CCD detector.[48] For $EuCl_3$, the fructose ROA/CPL spectral pattern is much simpler and the signal is weaker (dominated by 1823 (−) and 2055 (+) cm^{-1} bands) than for EuEDTA. For mannose, the situation is rather opposite; i.e., there is a strong, about six-band signal with $EuCl_3$ and a weaker 1808(+)/1888(−) cm^{-1} "couplet" (two strong close bands of similar intensities but of opposite signs)

DOI: 10.1021/acs.analchem.6b02505
Anal. Chem. 2016, 88, 8878−8885

dominating the EuEDTA spectrum. The third EuDEPA complex gives much weaker CPL for both sugars.

Glucose and galactose are rather similar in that their CPL is about 10× weaker than for fructose and mannose, although the luminescence is still significantly stronger than the vibrational ROA. Also, in terms of CID, the highest values are provided by mannose/$EuCl_3$ (~3×10^{-3}) and fructose/EuEDTA or $EuCl_3$ complexes (~1×10^{-3}), while CID values for glucose and galactose are smaller than 2×10^{-4}. However, the "performance" of the EuDEPA complex for glucose and galactose is better than for fructose and mannose, as it provides CPL intensities comparable to EuEDTA.

Typical Raman spectra for fructose are plotted in Figure 3; spectra of the other sugars are quite similar and can be found in

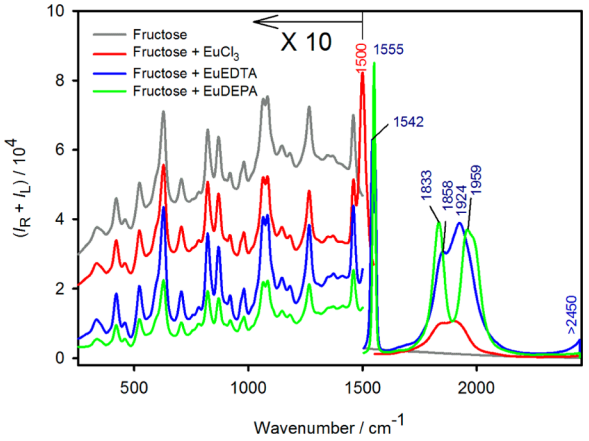

Figure 3. Raman spectra of $EuCl_3$, EuEDTA, and EuDEPA solutions in the presence of fructose. The Raman/luminescence spectra are not as sensitive to the sugar type as CPL.

the Supporting Information. As for ROA, the 200−1500 cm^{-1} region is dominated by a relatively weak vibrational Raman scattering of the sugar, whereas above 1500 cm^{-1}, the spectrum mostly comprises the total luminescence of europium. The Raman spectrum obviously also comprises the luminescence, and intensities of both are not much affected by the presence of monosaccharides. This reflects the generally lower sensitivity of unpolarized spectra to structural changes[16] and weak binding interactions between the europium ions/complexes and the sugars. On the other hand, $EuCl_3$, EuEDTA, and EuDEPA do exhibit specific luminescence. For example, $EuCl_3$ provides the weakest signal around 1900 and 1500 cm^{-1}; the latter transition is also shifted to higher wavenumbers for the other two complexes. EuDEPA gives the most characteristic split luminescence bands at 1833/1959 cm^{-1}.

Ligand Filed Theory Simulations. Luminescence spectra of the europium(III) ion in $Eu(H_2O)_9$ cluster and EuDEPA and EuEDTA optimized geometries, as simulated by the ligand (crystal) field theory, are plotted in Figure 4. The accuracy of the semiempirical approach is limited; for example, the experimental bands observed within 1860−1930 cm^{-1} are predicted at 1630−1790 cm^{-1} etc., and even bigger error is expected for the intensities. However, the model provides a solid basis for the band assignment. It is based on energy levels of free Eu^{3+} ion, because even in crystals and complexes, the orbital (L), spin (S), and total (J) quantum numbers are not quenched.[49] Using the usual notation $^{2S+1}L_J$, we can thus distinguish the $^5D_1 \rightarrow {}^7F_2$ (experimentally at 650−1010 cm^{-1}/

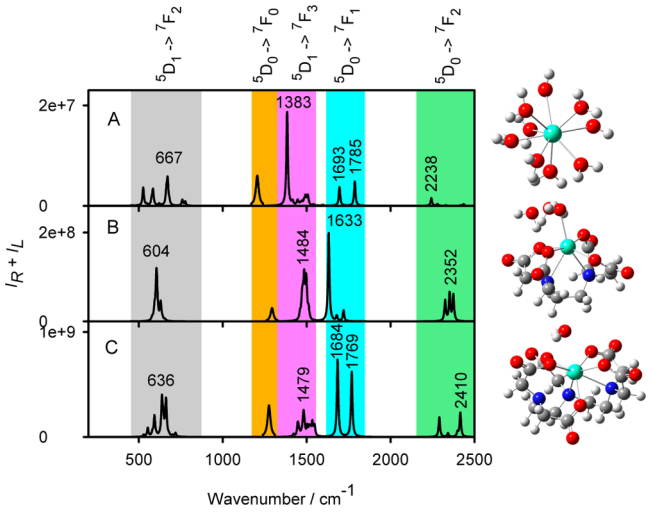

Figure 4. Simulated Raman/luminescence spectra of a $Eu(H_2O)_9$ cluster, EuEDTA, and EuDEPA ions. The $^5D_0 \rightarrow {}^7F_0$ bands were multiplied by 100 to be visible. The ligand (crystal)-field theory enables one to identify observed transitions.

calculated at 570−680 cm^{-1}), $^5D_1 \rightarrow {}^7F_3$ (1500−1550/1460−1510), $^5D_0 \rightarrow {}^7F_1$ (1860−1930/1630−1790), and $^5D_0 \rightarrow {}^7F_2$ (>2400/2300−2400) regions, in agreement with europium energies observed in other systems.[12] Even some experimentally observed intensity trends are predicted by this model, such as the lower intensity of the $^5D_0 \rightarrow {}^7F_1$ transitions of the hydrated Eu^{3+} ion compared to EuEDTA and EuDEPA, smaller signal of $^5D_1 \rightarrow {}^7F_3$ fluorescence in EuDEPA than in EuEDTA, and the split and shift of the EuDEPA $^5D_0 \rightarrow {}^7F_1$ bulk intensity toward higher wavenumbers compared to EuEDTA.

On a *qualitative* level, the crystal field theory can thus be used to simulate the CPL intensities stemming from the Eu^{3+} ion and reveal the chirality-induction mechanism. The spectra of europium complexes with the EDTA and DEPA ions and with α- and β-mannose are plotted in Figure 5. The mannose

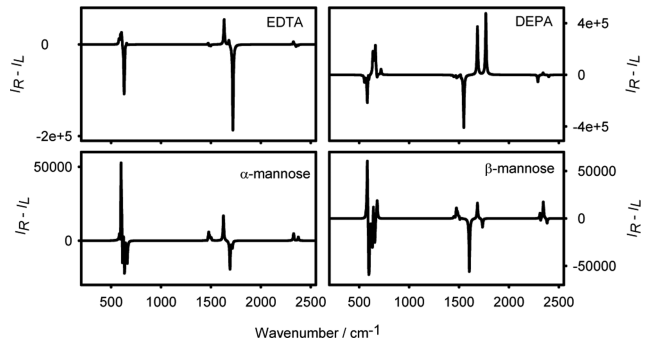

Figure 5. Simulated ROA/CPL spectra of Eu^{3+} complexes with EDTA, DEPA, and α- and β-mannose. The ligand-field theory qualitatively describes the experimental observations.

complexes were chosen as their geometry maximizes the number of Eu···O interactions. Note that the EuEDTA and DEPA complexes are chiral; in solution, they exist in an equilibrium of the "Δ" and "Λ" enantiomeric forms.[29,30]

The simulations are well consistent with the experiment in that the predicted CID ratios (2×10^{-4} to 1×10^{-3}) agree with the experimental range of dissymmetry factors found for the EDTA and DEPA complexes and bare Eu^{3+} ion. The CPL/total

DOI: 10.1021/acs.analchem.6b02505
Anal. Chem. 2016, 88, 8878−8885

Table 1. Fluorescence Decay Times (t_1 and t_2, in μs) and Relative Amplitudes (A_1 and A_2, in %) of Three Bands (around 592, 615, and 697 nm, Exact Peak Positions λ_{max} in nm) as Obtained by a Two-Exponential Fit $I = I_0 + A_1 \exp(-t/t_1) + A_2 \exp(-t/t_2)$[a]

	~592 nm					~615 nm					~697 nm				
	λ_{max}	t_1	t_2	A_1	A_2	λ_{max}	t_1	t_2	A_1	A_2	λ_{max}	t_1	t_2	A_1	A_2
$EuCl_3$	591.6	106	1430	85	15	615.8	100	1697	79	21	697.7	98	1933	77	23
$EuCl_3$+F[b]	591.6	101	384	73	27	615.8	98	474	75	25	696.9	82	866	69	31
$EuCl_3$+M[b]	591.2	105	459	75	25	615.8	103	462	69	32	695.9	113	516	71	29
EuEDTA	592.5	210	732	56	44	615.5	249	613	53	37	697.5	147	818	42	58
EuEDTA+F[b]	592.8	57	355	12	88	615.4	70	343	8	92	698.3	874	481	29	71
EuEDTA+M[b]	592.9	130	475	33	67	615.8	18	304	7	93	698.2	58	434	33	67
EuDEPA	594.5	110	745	11	89	615.4	158	708	8	92	694.8	97	796	12	88
EuDEPA+F[b]	594.2	41	603	17	83	615.2	35	572	9	91	694.8	37	563	21	79
EuDEPA+M[b]	594.2	104	766	13	87	615.5	135	717	9	91	695.1	89	817	14	86

[a]The excitation wavelength was 405 nm. [b]F, fructose; M, mannose.

fluorescence ratio is predicted much more reliably than the actual intensities, because absolute values of the transition moments are not known.[36,37] The plausible mechanisms of the chirality transfer involve the previously suggested perturbation of the $\Delta \leftrightarrow \Lambda$ equilibrium by a preferential binding to the sugar[11] but also a direct Eu^{3+}–sugar interaction. The comparable CPL intensities for all the systems in Figure 5 show that both mechanisms are possible, which is also consistent with the observations of high induced chirality, in both the complexes and bare (hydrated) Eu^{3+} ion (Figure 3). However, the actual mode of interaction of EuEDTA, DEPA, and Eu^{3+} with the sugars may all be similar also because the europium ion makes relatively stable aggregates with water. To some extent, its first solvation sphere thus behaves as a complex, too.[50,51]

Fluorescence Decay Times. The fluorescence decay times were determined for the most strongly interacting sugars, fructose and mannose. The times are summarized in Table 1 for the fluorescence at 590 nm. They are relevant for the most pronounced ROA/CPL signal at ~1850 cm^{-1} and confirm specificity of the interactions. All decay curves could be well fitted by a double-exponential function. Compared to typical organic molecules, rather long fluorescence times are observed, unique for the lanthanide electronic system and mostly involving the *f*-shell europium electronic levels.[12]

For example, the addition of mannose or fructose to $EuCl_3$ and EDTA shortens the decay times (in particular t_2), and the amplitude of the longer-time component (A_2) rises. This effect is significantly stronger for fructose than for mannose. The fluorescence kinetics of the DEPA complex is rather unperturbed by mannose, but there is some effect of fructose in shortening the shorter time t_1 from 110 to 41 μs and rising its amplitude A_2. This corresponds to the stronger chiroptical response of EDTA, as shown in Figure 2. The kinetic data including different fluorescence peaks are summarized in Figure 6 revealing similar sensitivity and specificity to the lanthanide–sugar interactions across the entire spectrum.

NMR Chemical Shift Changes. The chemical shifts induced in D_2O solutions of mannose and fructose by $EuCl_3$ and EuEDTA also indicate selective interactions of the europium ion and complexes with the monosaccharides, even though they are not as specific as for the fluorescence. They suggest complex binding with multiple binding sites and a rather weak interaction. In general, the addition of a paramagnetic ion into the sample was accompanied by both

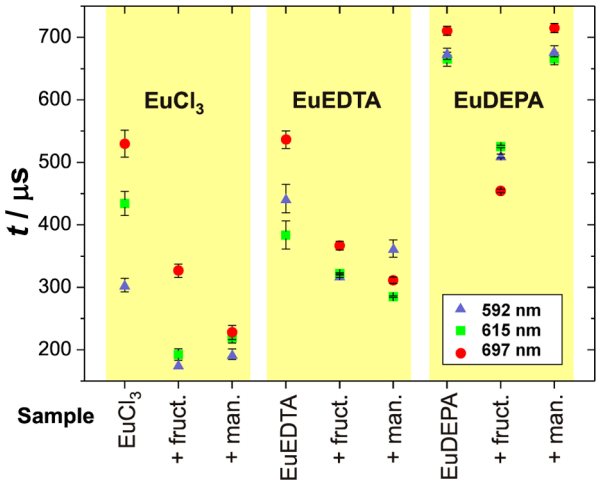

Figure 6. Average fluorescence decay times ($t = A_1 t_1 + A_2 t_2$) at three different wavelengths for the three europium compounds, with and without sugars.

line broadening (due to enhanced "T_2" relaxation) and chemical shift changes.

Assignment of the proton spectra was impossible because the monosaccharide solutions contained two (α/β mannose anomers) or four (α/β anomers for each furanose and pyranose fructose form) sugar isomers, most of the ^1H signals clustered in a very narrow chemical shift range (3.2–4.0 ppm), and after the addition of europium compounds the lines became too broad to be assignable. Therefore, we focused on ^{13}C NMR spectra, where the signals were well separated in most cases, and the line broadening did not prevent signal assignment and interpretation. The signals were referenced to the C_6D_6 external standard (sealed in a capillary), i.e., europium-free.

Mannose exists in water solution as a mixture of α- and β-D-mannopyranose in a ratio of about 2:1. Both the $EuCl_3$ and EuEDTA solutions caused a downfield shift (higher chemical shift values) of all mannose ^{13}C signals. The chemical shift change is almost uniform across all carbon atoms (1 ppm for 2:1 ratio of mannose–$EuCl_3$ and about 0.5 ppm for the same stoichiometric mixture of mannose–EuEDTA), which may suggest that there is not a single strongly preferred geometry of the metal–sugar interaction. A typical dependence of relative chemical shifts on europium concentration is exemplified in Figure 7 for the C3 carbon atom. A closer look, however,

DOI: 10.1021/acs.analchem.6b02505
Anal. Chem. 2016, 88, 8878–8885

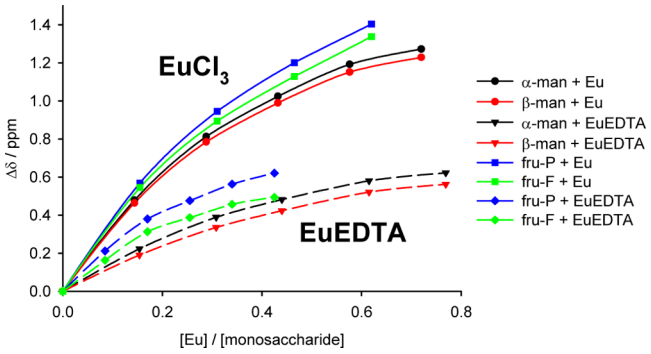

Figure 7. Changes of ^{13}C chemical shifts ($\Delta\delta$) of carbon C3 in mannose and fructose, upon addition of $EuCl_3$ and EuEDTA: α-man, α-D-mannopyranose; β-man, β-D-mannopyranose; fru-P, β-D-fructopyranose; fru-F, β-D-fructofuranose. The variations are small relative to the overall shift but specific for a particular sugar or carbon type.

reveals that the chemical shift changes are not completely uniform and slight differences between individual carbon atoms exists. Interestingly, such differences between individual carbon atoms are much more pronounced for the interaction with EuEDTA complex, which may indicate that the specificity of the EuEDTA–sugar interaction is greater than for $EuCl_3$. It is true that the EuEDTA average chemical shift changes are about two times smaller than those caused by $EuCl_3$, but this is likely to be caused by the EDTA ligands, at least partially or fully preventing a direct europium–sugar binding.

At equilibrium, fructose in water solution is present as a mixture of two predominant forms (70% of β-D-fructopyranose and 21% of β-D-fructofuranose), together with two minor α-forms.[52] As for mannose, an addition either of $EuCl_3$ or EuEDTA caused a downfield shift of all fructose ^{13}C signals. Interestingly, differences between individual chemical shift changes induced by $EuCl_3$ were much higher for the pyranose rather than the furanose form (Figure 8), which indicates that the pyranose–europium interaction may be linked to a more distinct complex structure. The addition of EuEDTA led to significantly broader carbon signals (particularly C2, C4, C5, and C6 in β-D-fructopyranose; C1, C2, and C4 in β-D-fructofuranose) than did similar amounts of added $EuCl_3$, indicating a stronger binding of the former. The NMR spectra

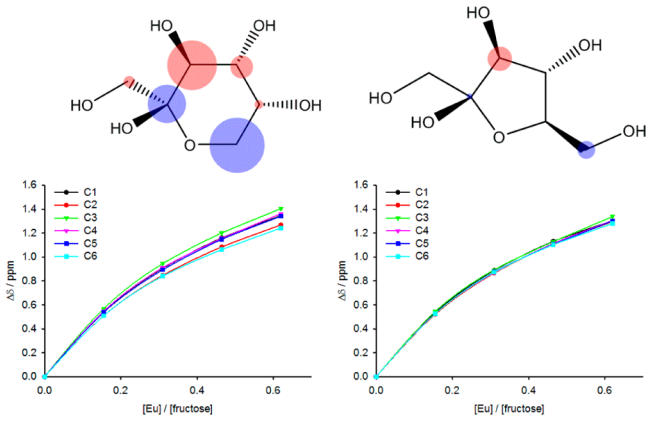

Figure 8. ^{13}C chemical shifts changes ($\Delta\delta$) of carbon atoms in β-D-fructopyranose (left) and in β-D-fructofuranose (right), as caused by the addition of $EuCl_3$. Relative deviations from the average shift change are indicated for all carbons by disks of different diameters (positive, red; negative, blue) in the structures.

thus confirmed the specificity of the europium compounds–sugar interactions and suggested a weak, multisite binding.

MD Modeling of the Europium–Sugar Interactions. Currently, we find it too difficult to reliably simulate all aspects of interactions of the larger EuEDTA and EuDEPA complexes with the monosaccharides. However, for the free europium ion, the MD simulations do reveal the basic binding patterns and energy changes associated with the complexation. The formation free energies of most favored geometries listed in Table 2 suggest that the complexes are rather unstable; the

Table 2. Free Energies of the Sugar–Eu^{3+} Complex Formation, As Calculated Using the Molecular Dynamics and the WHAM Method

sugar	isomer	oxygens bound to Eu	ΔG (kcal/mol)
α-fructopyranose	af1	O_3 O_4	1.0
	af2	O_1 O_3 O_6	1.0
	af3	O_2 O_4 O_5 O_6	0.95
	af4	O_1 O_2 O_6	0.6
β-fructopyranose	bf1	O_1 O_4 O_5 O_6	1.0
	bf2	O_2 O_3 O_6	1.0
	bf3	O_1 O_2 O_6	0.75
α-fructofuranose	cf1	O_1 O_3 O_6	0.9
	cf2	O_2 O_4 O_5	0.8
	cf3	O_1 O_5 O_6	0.7
	cf4	O_1 O_2 O_5	0.6
β-fructofuranose	df1	O_2 O_3 O_6	1.1
	df2	O_1 O_2 O_3	0.9
	df3	O_1 O_2 O_6	0.8
α-mannose	am1	O_1 O_5 O_6	0.9
	am2	O_1 O_2	0.8
	am3	O_2 O_3	0.7
	am4	O_2 O_5 O_6	0.5
β-mannose	bm1	O_1 O_2 O_5 O_6	0.9
	bm2	O_2 O_3	0.9

biggest stabilization energies (~1 kcal/mol) are comparable with the Boltzmann temperature quantum (~0.6 kcal/mol at 300 K). In addition, many approximately equally convenient binding sites are possible at ambient temperature, which is well in agreement with the NMR data discussed above, and binding to more hydrogen atoms often does not yield a more stable complex.

The process of complex formation can also be understood on the whole profiles of the mean force potentials (free energies) obtained by the WHAM method. They are quite similar (Figure S6), and the lowest-energy isomer of the β-fructopyranose/Eu^{3+} complex was selected as an example in Figure 9. Here, we can see a free (IV) and weakly stabilized (~0.2 kcal/mol) preassociation state (III) of the hydrated europium ion surrounded by nine water molecules. The actual binding to the sugar requires a destruction of this hydration shell, which is associated with a relatively high energy (~1 kcal/mol) of the transition state (II). Finally, the most stable complex (I) is stabilized, by about 1 kcal/mol.

Because of the high energy needed to break the europium hydration shell, the bound state (I in Figure 9) could not be obtained from free dynamics in a reasonable time. However, the more weakly associated states (III, essentially a complex of the sugar and $[Eu(H_2O)_9]^{3+}$ ion) are visible in the europium probability plot based on free MD. In the example for β-D-

DOI: 10.1021/acs.analchem.6b02505
Anal. Chem. 2016, 88, 8878–8885

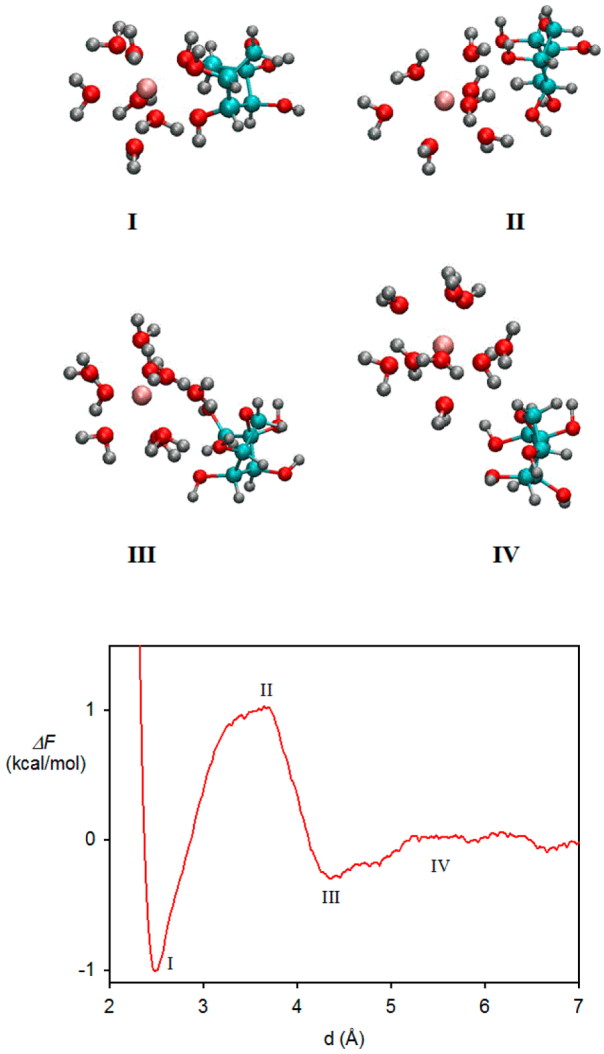

Figure 9. Typical WHAM free energy profile for sugar−europium(III) binding (this one for *β*-fructopyranose) and an example of geometries along the reaction coordinates. The complex formation requires the europium hydration shell to be disturbed, which is associated with a relatively high activation energy.

fructopyranose in Figure 10, we can see that also for this interaction preferential sites exist.

For the direct Eu−sugar complexes (I), the equilibrium Eu···O distance of ∼2.4 Å agrees well with available crystallographic data.[3,4] Geometries of the most stable complexes of various

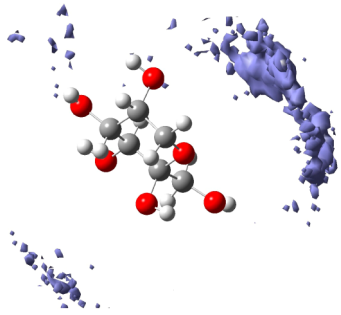

Figure 10. Regions of highest density of the Eu^{3+} ion obtained from a 300 ns molecular dynamics run with *β*-D-fructopyranose corresponding to part III in Figure 9.

fructose and mannose forms are plotted in Figure 11, and their variability is thus consistent with the rich spectroscopic responses.

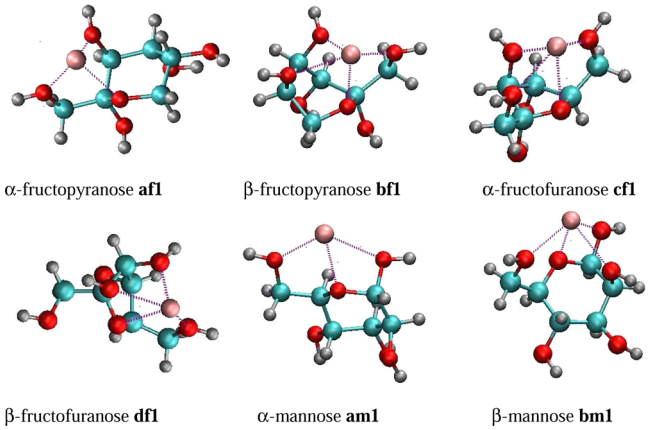

Figure 11. Some lowest-energy conformers of fructose and mannose complexes with Eu^{3+} (cf. Table 2).

CONCLUSIONS

We have explored the interaction of europium compounds with common monosaccharides using ROA/CPL, time-dependent luminescence and NMR spectroscopies. Very specific spectral patterns have been observed for the circularly polarized luminescence, for both the sugar and europium components. The complexation specificity of the spectral response was confirmed by measurement of the fluorescence decay times. In NMR spectra, the paramagnetic lanthanide metal caused nearly uniform chemical shift of the sugar carbon atoms; finer relative shift changes, however, were also very specific to the lanthanide compound and monosaccharide type. The luminescence/CPL spectral bands could be assigned and semiqualitatively modeled using the crystal field theory. Combined, the NMR experiment and molecular dynamics simulations suggest that multiple binding modes for each sugar form are possible, although the link between the actual geometry and detailed spectral data, especially for the interaction of the EDTA and DEPA complexes, still awaits elucidation. The ROA/CPL methodology appears to be a handy tool for studies of structure and interactions of sugars, requiring their identification and detection.

ASSOCIATED CONTENT

Supporting Information

The Supporting Information is available free of charge on the ACS Publications website at DOI: 10.1021/acs.analchem.6b02505.

Further experimental and computational details (PDF)

AUTHOR INFORMATION

Corresponding Authors

*E-mail: bour@uochb.cas.cz.

*E-mail: jan.valenta@mff.cuni.cz.

Notes

The authors declare no competing financial interest.

DOI: 10.1021/acs.analchem.6b02505
Anal. Chem. 2016, 88, 8878−8885

■ ACKNOWLEDGMENTS

The work was supported by the Grant Agency of the Czech Republic (16-05935S, 16-08764Y, 15-11223S, and 15-09072S).

■ REFERENCES

(1) Striegler, S.; Dittel, M. *J. Am. Chem. Soc.* **2003**, *125*, 11518.
(2) Davis, A. P.; Wareham, R. S. *Angew. Chem., Int. Ed.* **1999**, *38*, 2978.
(3) Yang, L.; Su, Y.; Xu, Y.; Zhang, S.; Wu, J.; Zhao, K. *J. Inorg. Biochem.* **2004**, *98*, 1251.
(4) Guo, J.; Lu, Y. *J. Carbohydr. Chem.* **2010**, *29*, 10.
(5) Yang, L.; Hua, X.; Xue, J.; Pan, Q.; Yu, L.; Li, W.; Xu, Y.; Zhao, G.; Liu, L.; Liu, K.; Chen, J.; Wu, J. *Inorg. Chem.* **2012**, *51*, 499.
(6) Alptürk, O.; Rusin, O.; Fakayode, S. O.; Wang, W.; Escobedo, J. O.; Warner, I. M.; Crowe, W. E.; Král, V.; Pruet, J. M.; Strongin, R. M. *Proc. Natl. Acad. Sci. U. S. A.* **2006**, *103*, 9756.
(7) Battistini, E.; Mortillaro, A.; Aime, S.; Peters, J. A. *Contrast Media Mol. Imaging* **2007**, *2*, 163.
(8) Lu, Y.; Deng, G.; Miao, F.; Li, Z. *Carbohydr. Res.* **2003**, *338*, 2913.
(9) Wang, W.; Gao, X.; Wang, B. *Curr. Org. Chem.* **2002**, *6*, 1285.
(10) Crescenzi, V.; Brittainc, H. G.; Yoshinoc, N.; Okamoto, Y. *J. Polym. Sci., Polym. Phys. Ed.* **1985**, *23*, 437.
(11) Huskowska, E.; Riehl, J. P. *Inorg. Chem.* **1995**, *34*, 5615.
(12) Binnemans, K. *Coord. Chem. Rev.* **2015**, *295*, 1.
(13) Riehl, J. P.; Muller, G. In *Comprehensive chiroptical spectroscopy, volume 1: Instrumentation, methodologies, and theoretical simulations*; Berova, N., Polavarapu, P. L., Nakanishi, K., Woody, R. W., Eds.; John Wiley & Sons: Hoboken, NJ, 2012; Vol. *1*, p 65.
(14) Wu, T.; Kapitán, J.; Mašek, V.; Bouř, P. *Angew. Chem., Int. Ed.* **2015**, *54*, 14933.
(15) Hug, W. *Appl. Spectrosc.* **2003**, *57*, 1.
(16) Nafie, L. *Vibrational optical activity: Principles and applications*; Wiley: Chichester, 2011.
(17) Barron, L. D. *Biomed. Spectrosc. Imaging* **2015**, *4*, 223.
(18) Johannessen, C.; Pendrill, R.; Widmalm, G.; Hecht, L.; Barron, L. D. *Angew. Chem., Int. Ed.* **2011**, *50*, 5349.
(19) Zhu, F.; Isaacs, N. W.; Hecht, L.; Barron, L. D. *J. Am. Chem. Soc.* **2005**, *127*, 6142.
(20) Melcrová, A.; Kessler, J.; Bouř, P.; Kaminský, J. *Phys. Chem. Chem. Phys.* **2016**, *18*, 2130.
(21) Zielinski, F.; Mutter, S. T.; Johannessen, C.; Blanch, E. W.; Popelier, P. L. A. *Phys. Chem. Chem. Phys.* **2015**, *17*, 21799.
(22) Barron, L. D. *Molecular Light Scattering and Optical Activity*; Cambridge University Press: Cambridge, 2004.
(23) Šugar, J.; Bouř, P. *J. Raman Spectrosc.* **2016**, DOI: 10.1002/jrs.4960, in press.
(24) Gawryszewska, P.; Legendziewicz, J.; Ciunik, Z.; Esfandiari, N.; Muller, G.; Piguet, C.; Cantuel, M.; Riehl, J. P. *Chirality* **2006**, *18*, 406.
(25) Moussa, A.; Pham, C.; Bommireddy, S.; Muller, G. *Chirality* **2009**, *21*, 497.
(26) Nguyen, B. T.; Ingram, A. J.; Muller, G. *Chirality* **2016**, *28*, 325.
(27) Valenta, J.; Greben, M. *AIP Adv.* **2015**, *5*, 047131.
(28) Frisch, M. J.; Trucks, G. W.; Schlegel, H. B.; Scuseria, G. E.; Robb, M. A.; Cheeseman, J. R.; Scalmani, G.; Barone, V.; Mennucci, B.; Petersson, G. A.; Nakatsuji, H.; Caricato, M.; Li, X.; Hratchian, H. P.; Izmaylov, A. F.; Bloino, J.; Zheng, G.; Sonnenberg, J. L.; Hada, M.; Ehara, M.; Toyota, K.; Fukuda, R.; Hasegawa, J.; Ishida, M.; Nakajima, T.; Honda, Y.; Kitao, O.; Nakai, H.; Vreven, T.; Montgomery, J.; Peralta, J. E.; Ogliaro, F.; Bearpark, M.; Heyd, J. J.; Brothers, E.; Kudin, K. N.; Staroverov, V. N.; Kobayashi, R.; Normand, J.; Raghavachari, K.; Rendell, A.; Burant, J. C.; Iyengar, S. S.; Tomasi, J.; Cossi, M.; Rega, N.; Millam, J. M.; Klene, M.; Knox, J. E.; Cross, J. B.; Bakken, V.; Adamo, C.; Jaramillo, J.; Gomperts, R.; Stratmann, R. E.; Yazyev, O.; Austin, A. J.; Cammi, R.; Pomelli, C.; Ochterski, J. W.; Martin, R. L.; Morokuma, K.; Zakrzewski, V. G.; Voth, G. A.; Salvador, P.; Dannenberg, J. J.; Dapprich, S.; Daniels, A. D.; Farkas, O.; Foresman, J. B.; Ortiz, J. V.; Cioslowski, J.; Fox, D. J.; *Gaussian 09*, Revision D01 ed.; Gaussian, Inc.: Wallingford CT, 2009.
(29) Gao, J. Q.; Wu, T.; Wang, J.; Bai, Y.; Wang, S. J.; Xu, Y. N.; Li, Y.; Zhang, X. D. *Russ. J. Coord. Chem.* **2012**, *38*, 491.
(30) Mondry, A.; Janicki, R. *Dalton Trans.* **2006**, 4702.
(31) Becke, A. D. *J. Chem. Phys.* **1993**, *98*, 5648.
(32) Figgen, D.; Rauhut, G.; Dolg, M.; Stoll, H. *Chem. Phys.* **2005**, *311*, 227.
(33) Scalmani, G.; Frisch, M. J. *J. Chem. Phys.* **2010**, *132*, 114110.
(34) Carnall, W. T.; Goodman, G. L.; Rajnak, K.; Rana, R. S. *J. Chem. Phys.* **1989**, *90*, 3443.
(35) Edvardsson, S.; Åberg, D. *Comput. Phys. Commun.* **2001**, *133*, 396.
(36) Judd, B. R. *Phys. Rev.* **1962**, *127*, 750.
(37) Ofelt, G. S. *J. Chem. Phys.* **1962**, *37*, 511.
(38) Richardson, F. S.; Faulkner, T. R. *J. Chem. Phys.* **1982**, *76*, 1595.
(39) Case, D. A.; Cheatham, I. T. E.; Darden, T.; Gohlke, H.; Luo, R.; Merz, J. K. M.; Onufriev, A.; Simmerling, C.; Wang, B.; Woods, R. *J. Comput. Chem.* **2005**, *26*, 1668.
(40) Kirschner, K. N.; Yongye, A. B.; Tschampel, S. M.; Outeiriño, J. G.; Daniels, C. R.; Foley, B. L.; Woods, R. J. *J. Comput. Chem.* **2008**, *29*, 622.
(41) Baaden, M.; Burgard, M.; Boehme, C.; Wipff, G. *Phys. Chem. Chem. Phys.* **2001**, *3*, 1317.
(42) Kumar, S.; Bouzida, D.; Swendsen, R. H.; Kollman, P. A.; Rosenberg, J. M. *J. Comput. Chem.* **1992**, *13*, 1011.
(43) Roux, B. *Comput. Phys. Commun.* **1995**, *91*, 275.
(44) Barron, L. D.; Gargaro, A. R.; Wen, Z. Q. *Carbohydr. Res.* **1991**, *210*, 39.
(45) Bell, A. F.; Hecht, L.; Barron, L. D. *J. Raman Spectrosc.* **1993**, *24*, 633.
(46) Cheeseman, J. R.; Shaik, M. S.; Popelier, P. L. A.; Blanch, E. W. *J. Am. Chem. Soc.* **2011**, *133*, 4991.
(47) Wen, Z. Q.; Barron, L. D.; Hecht, L. *J. Am. Chem. Soc.* **1993**, *115*, 285.
(48) Profant, V.; Pazderková, M.; Pazderka, T.; Maloň, P.; Baumruk, V. *J. Raman Spectrosc.* **2014**, *45*, 603.
(49) Walrand, C. G.; Binnemans, K. In *Handbook on the physics and chemistry of rare earths*; Gschneider, K. A., Eyring, L., Eds.; Elsevier Science B. V.: Amsterdam, 1996; p 121.
(50) Chaussedent, S.; Monteil, A. *J. Chem. Phys.* **1996**, *105*, 6532.
(51) Clavaguéra, C.; Pollet, R.; Soudan, J. M.; Brenner, V.; Dognon, J. P. *J. Phys. Chem. B* **2005**, *109*, 7614.
(52) Barclay, T.; Ginic-Markovic, M.; Johnston, M. R.; Cooper, P.; Petrovsky, N. *Carbohydr. Res.* **2012**, *347*, 136.

DOI: 10.1021/acs.analchem.6b02505
Anal. Chem. 2016, 88, 8878−8885